Progress in Nuclear Energy 52 (2010) 76–83

Contents lists available at ScienceDirect

Progress in Nuclear Energy

journal homepage: www.elsevier.com/locate/pnucene

Simulation of corium concrete interaction in 2D geometry

Michel Cranga [a,*], Bertrand Spindler [b], Emmanuelle Dufour [b], Dimitar Dimov [c], Kresna Atkhen [d], Jerzy Foit [e], Monica Garcia-Martin [f], Tuomo Sevon [g], Werner Schmidt [h], Claus Spengler [i]

[a] Institut de Radioprotection et de Sûreté Nucléaire (IRSN), DPAM – Bat 702, BP 3, 13115 St-Paul-Lez-Durance Cedex, France
[b] Commissariat à l'Energie Atomique (CEA), DEN, F-38000 Grenoble, France
[c] Institut for Nuclear Research and Nucler Energy (INRNE), NPPSAL, 72 Blvr Tzarigradsko chaussee, 1748 Sofia, Bulgaria
[d] Electricité de France (EDF), SEPTEN,12-14 Av. Dutrievoz, Villeurbanne, 7 N: F-69628, France
[e] Forschungzentrum Karlsruhe (FZK) GmbH, Postfach 3640, 76021 Karlsruhe, Germany
[f] Universidad Politecnica de Madrid(UPM), C/José Gutierrez Abascal, 2–28006, Madrid, Spain
[g] Technical Research Centre of Finland (VTT), P.O.Box 1000, FI-02044, Finland
[h] AREVA, Freyeslebenstrasse 1, 91058 Erlangen, Germany
[i] Gesellschaft für Anlagen und Reaktorsicherheit (GRS) mbH, Schwertnergasse 1, 50667 Köln, Germany

Keywords:
MCCI
Codes
Benchmarking
Reactor cases

A B S T R A C T

Benchmarking work was recently performed for the issue of molten corium concrete interaction (MCCI). A synthesis is given here. It concerns first the 2D CCI-2 test with a homogeneous pool and a limestone concrete, which was used for a blind benchmark. Secondly, the COMET-L2 and COMET-L3 2D experiments in a stratified configuration were used as a post-test (L2) and a blind-test (L3) benchmark. More details are given here for the recent benchmark considering a matrix of four reactor cases, with both a homogeneous and a stratified configuration, and with both a limestone and a siliceous concrete. A short overview is given on the different models used in the codes, and the consistency between the benchmark actions on experiments and reactor situations is discussed. Finally, the major uncertainties concerning MCCI are also pointed out.

1. Introduction

In the hypothetical event of a severe accident in a Light Water Reactor, corium, a mixture of molten materials issued from the fuel, cladding and structural elements, may appear in the reactor core. In some scenarios, corium is assumed to melt through the reactor pressure vessel and spread over the concrete basemat of the reactor pit. Molten Core Concrete Interaction (MCCI) then occurs, characterized by concrete ablation. The main question that has to be addressed is whether and when the corium will make its way through the basemat since it would lead to a failure of the containment. The MCCI phenomena occurring in case of an oxide corium pool have been largely investigated but uncertainties still remain. The main remaining issues are on one hand the partition between lateral and axial ablation in a mixed pool, and on the other hand the ablation behaviour in a stratified pool with oxide and metallic layers.

An overview of the models included in the principal codes is first given, with emphasis on the interfacial conditions at the bottom and side walls on one hand, and at the interface between two stratified layers on the other hand. Then, some recent 2D experimental data are presented, and the corresponding benchmarks results are discussed. A subsequent part describes benchmark results from reactor calculations performed for different pool configurations and for two concrete types. Finally, MCCI sub-items requiring additional investigations on experimental and modelling aspects are pointed out.

2. Codes and models

A detailed review of the MCCI models and codes was recently made (Allelein and Bürger, 2006). A short presentation of the codes was also given in a paper presenting the COMET-L2-L3 benchmark (Spindler et al., 2007a). Hence only some elements are given here: in Table 1 the list of organisations with codes used for the different benchmarks and references; in Table 2 main features of models and assumptions used in the codes in particular for heat transfer phenomena.

3. The CCI-2 benchmark

The benchmarking work concerning CCI-2 test (Farmer et al., 2005) was performed within the OECD-MCCI project. The results are not yet open. They were presented at a MCCI Project seminar

* Corresponding author. Tel.: +33 442199482; fax: +33 442199167.
E-mail address: michel.cranga@irsn.fr (M. Cranga).

0149-1970/$ – see front matter © 2009 Elsevier Ltd. All rights reserved.
doi:10.1016/j.pnucene.2009.09.016

Table 1
Codes used in the different benchmarks with reference for the code description.

Organisation	Code	Reference	CCI-2 benchmark	COMET-L2-L3 benchmark	Reactor benchmark
AREVA	COSACO	(Nie et al., 2002)	X	X	
CEA	TOLBIAC-ICB	(Spindler et al., 2006)	X	X	X
EDF	TOLBIAC-ICB	(Spindler et al., 2006)	X	X	
FZK	WECHSL	(Foit, 1997)		X	X
GRS	ASTEC/MEDICIS	(Cranga et al., 2005)	X	X	X
GRS	WEX	(Langhans et al., 2001)	X	X	
IRSN	ASTEC/MEDICIS	(Cranga et al., 2005)	X	X	X
UPM	MELCOR	(Gauntt et al., 2005)		X	X
VTT	MELCOR	(Gauntt et al., 2005)		X	
VTT	CORQUENCH	(Farmer, 2001)			X

(Spindler et al., 2007b). The most interesting results concerning code comparisons are the blind calculations performed before the experiment. They were performed with the same data for all participants. However, the final input data for the simulation of the experiment were significantly modified after the experiment (in particular melt mass involved in the interaction and concrete composition). Therefore, the comparison of the blind calculation results with the experimental results is of reduced interest, since some results highly depend on the melt composition. A comparison of the code results with the final input data was not organized. Only the results obtained by participants involved in the SARNET program are summarized here.

Very large temperature differences (Fig. 1a) are observed for the different codes, with three kinds of initial behaviour: sharp increase, gradual decrease and sharp decrease. This behaviour is related to the condition that is used for the heat transfer between melt and concrete. An interfacial temperature equal to the liquidus temperature gives an increase of the melt temperature because the initial temperature is lower than the calculated liquidus temperature. On the opposite, an interfacial temperature equal to the solidus temperature gives an initial decrease of the melt temperature. After about one hour, a regular evolution of the melt temperature is reached. At the time water is poured on the melt, a rapid decrease is observed in some codes.

The initial ablation rate differs depending on the code, and this discrepancy is connected to the melt temperature behaviour. After about one hour, the ablation rates are less dispersed (Fig. 1b). The final shape of the cavity mainly depends on the choice made by the code user: either isotropic heat transfer (which corresponds to what was observed in the experiment) or radial heat transfer higher than axial heat transfer.

4. The COMET-L2-L3 benchmark

4.1. COMET-L2 and L3 experiments

The COMET-L2 test (Sdouz et al., 2006) was performed at Forschungszentrum Karlsruhe in the frame of the LACOMERA project of the 5th European Framework Programme. The melt is composed with oxide (alumina and calcia) and metal (iron and nickel). The

Table 2
Codes main models and assumptions. WEX is based on the WECHSL code, with some modified models including new heat transfer coefficients.

Code	ASTEC/ MEDICIS by GRS	ASTEC/ MEDICIS by IRSN	COSACO	COR-QUENCH	MELCOR	TOLBIAC-ICB	WECHSL WEX
Heat transfer at concrete/pool side	correlation from exp. results	BALI (Bonnet, 2000) + slag layer	BALI	Kutateladze and Malenkov, 1978	slag layer	BALI	Depending on the existing gas flow
Heat transfer at concrete/pool bottom	correlation from exp. results	BALI + slag layer	BALI	(Kutateladze and Malenkov, 1978)	Kutate-ladze	BALI	Depending on the existing gas flow
Heat transfer at pool upper interface	correlation from exp. results	BALI	BALI	(Kutateladze and Malenkov, 1978)	Modified Kuta-teladze	BALI	Depending on the existing gas flow
Heat transfer at oxide/metal interface	(Greene and Irvine, 1988)	Greene	BALI	not used	Greene	BALI	(Werle, 1982)
Pool/crust interface temperature	$T_{solidus}$	$0.8\ T_{liquidus} + 0.2\ T_{solidus}$	not used in the model	$T_{solidus}$	$T_{solidus}$	$T_{liquidus}$	$T_{sol} \leq T_{int} \leq T_{liq}$
Crust composition Tsolidus and Tliquidus vs. oxide composition	pool composition (Roche et al., 1993)	pool composition NUCLEA data base (Cheynet et al., 2004)	Refracttory material COS-CHEM data base density	pool composition (Roche et al., 1993)	pool com-position assuming ideal solutions	Refracttory material NUCLEA data base	pool composition input data
Stratification criterion	not used	modified BALISE criterion	not used	not used	Specific model	BALISE criterion (Tourniaire et al., 2003)	not used

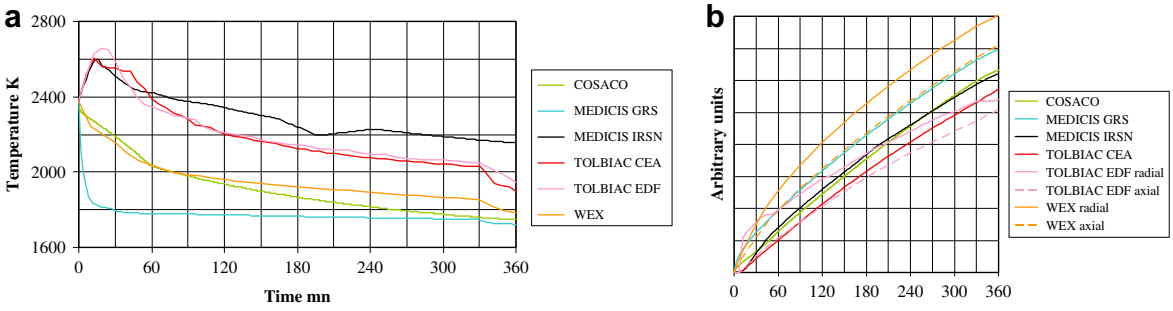

melt temperature versus time.

ablation depth versus time.

Fig. 1. CCI-2 benchmark.

heating power is concentrated in the bottom metal layer and was switched off automatically at 1015 s. The bottom flooding of the crucible started at 1440 s. The COMET-L3 test (Alsmeyer et al., 2007) differs from COMET-L2 mainly by a top flooding that occurs at 800 s. After an initial period of about 100 s until end of overheat, characterized by an isotropic and fast ablation, a steady state regime is reached, with a faster axial ablation compared to the lateral ablation (factor 2–3), which is in agreement with the results of the BETA experiments at a low power density (Foit, 2007).

A summary of the benchmark results is presented here. The detailed results are given in (Spindler et al., 2007a).

4.2. COMET-L2 benchmark results

The COMET-L2 test was used for a post test benchmark. The same input data were used by all the participants.

The scatter between the calculated metal temperatures (Fig. 2a) is about 150 K, but six results are between 1750 and 1780 K. The scatter between the oxide temperatures (Fig. 2b) is larger: about 450 K at 1000 s. There are no bulk temperature measurements for comparison. There is also a large scatter concerning the ablation depth (Fig. 2c and d), but it can be noticed that, after the first phase corresponding to the initial overheat, the ablation rate is similar for all the codes. Finally, when compared to the experimental results, it is found that the maximum axial ablation is underestimated.

4.3. COMET-L3 benchmark results

The COMET-L3 test was used for a blind-test benchmark: the experimental results were not known when the calculations were performed, but for some code, the model modifications tested in order to get a better agreement with COMET-L2 were used for the simulation of COMET-L3. The results are presented on Fig. 3.

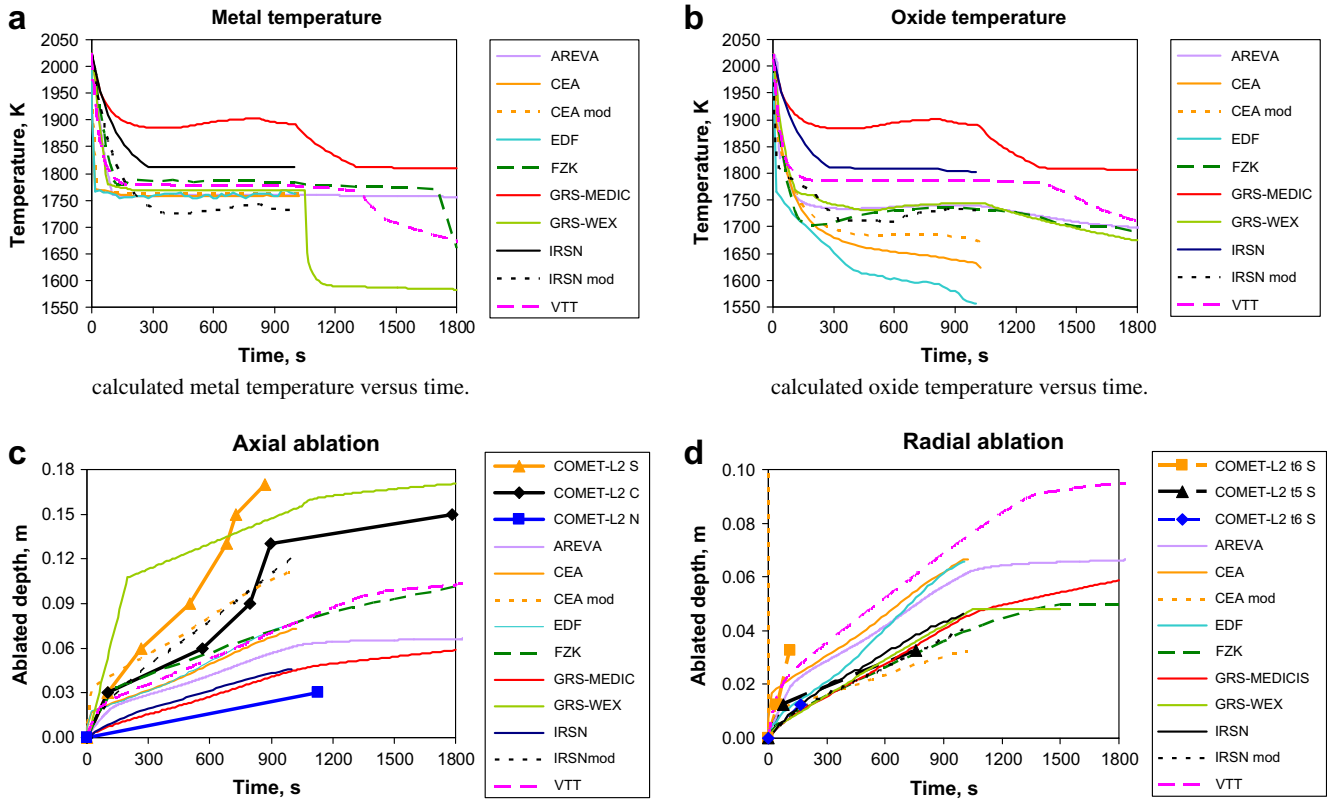

calculated metal temperature versus time.

calculated oxide temperature versus time.

calculated and measured axial ablation versus time.

calculated and measured lateral ablation versus time.

Fig. 2. COMET-L2 benchmark. CEA and IRSN presented a base calculation and calculations with a modified model for a better agreement with the experimental results.

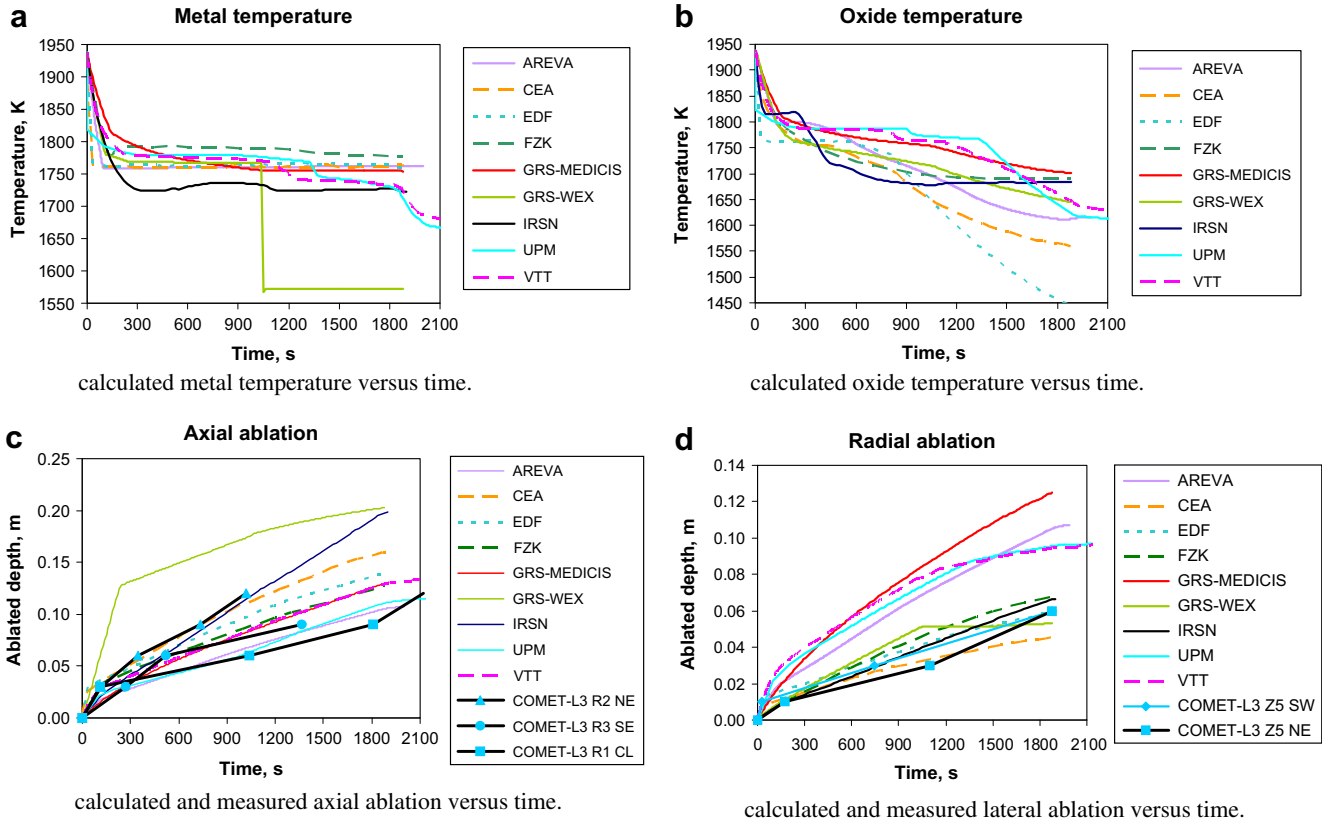

calculated metal temperature versus time.

calculated oxide temperature versus time.

calculated and measured axial ablation versus time.

calculated and measured lateral ablation versus time.

Fig. 3. COMET-L3 benchmark.

The top flooding at 800 s is sensitive for one calculated temperature only. It can be observed that the scatter of the calculated oxide and metal temperatures (Fig. 3a and b) is reduced compared to COMET-L2, because fitting of some parameters on COMET-L2. In the initial phase, some codes give a heat transfer from the oxide layer to the metal layer and the others from the metal to the oxide. In the second phase, before flooding, all codes predict heat transfer from the metal to the oxide. After flooding, some codes give back a heat transfer from the oxide to the metal.

For production of gas through oxidation of the metal layer (H_2 and CO) the scatter is large, with about a factor 5 between the larger and the lower values. There is also a large scatter concerning the ablation depth (Fig. 3c and d). Some codes give results which are similar to the experimental results. Some others overestimate the axial ablation or the lateral ablation, and the ablated volume.

5. The reactor benchmark

The wide range of predicted basemat failure times obtained in previous parametrical studies (Cranga et al., 2005, 2007), and also the benchmarking work concerning MCCI experiments, point out the interest of performing a reactor benchmark on the long term MCCI phase. The objectives are to compare code reactor results and to identify the major uncertainties in physical assumptions and models used in available codes. In this paper, more details are given on this reactor benchmarking work, in comparison to the two previous cases, because they have not yet been presented elsewhere.

5.1. Calculation conditions

A simplified geometry is used, with a cylindrical reactor pit of radius 3 m and basemat axial thickness 6 m. The lateral basemat thickness is assumed to be infinite: no limitation of lateral ablation before the axial melt-through is considered. The initial corium inventory in oxides and metals and the decay power evolution are typical of that of BWR. Two cases of pool configuration under dry conditions are considered: a fixed homogeneous pool and a case with a stratified configuration or with a configuration evolution. Two types of concretes are addressed: a siliceous concrete with 64% SiO_2, 18% CaO and 10% CO_2 weight fractions and a limestone concrete with 25% SiO_2, 42% CaO and 25% CO_2 weight fraction. The calculations are pursued until axial melt-through. A mass fraction of iron bars embedded in the concrete of 6.5% is taken into account in MCCI calculations.

5.2. Homogeneous pool, limestone concrete

Some results are presented in Fig. 4. The final temperature scatter is about 350 K (Fig. 4a). The use of a pool/crust interface temperature near the liquidus in IRSN and CEA calculations gives a melt temperature that increases after about 2 days, whereas a regular decrease is obtained for the other codes, with an interface temperature corresponding to the solidus. Such a long term increase of reactor pool temperature was not observed in relevant experiments such as CCI-2, and indeed the simulations of CCI-2 by CEA and IRSN show a decreasing temperature. The reason is the liquidus temperature versus pool composition, as given by GEMINI, which depends on the presence of magnesia (CCI-2) or not (present reactor case), and also increases at later times, after the eutectic composition of the corium-concrete mixture has been reached, due to the higher ablated concrete fraction reached in the reactor case but not in the CCI-2 experiment.

As far as concrete ablation is concerned (Fig. 4b), a reduced scattering is found up to a 4 m ablated axial depth reached at a time

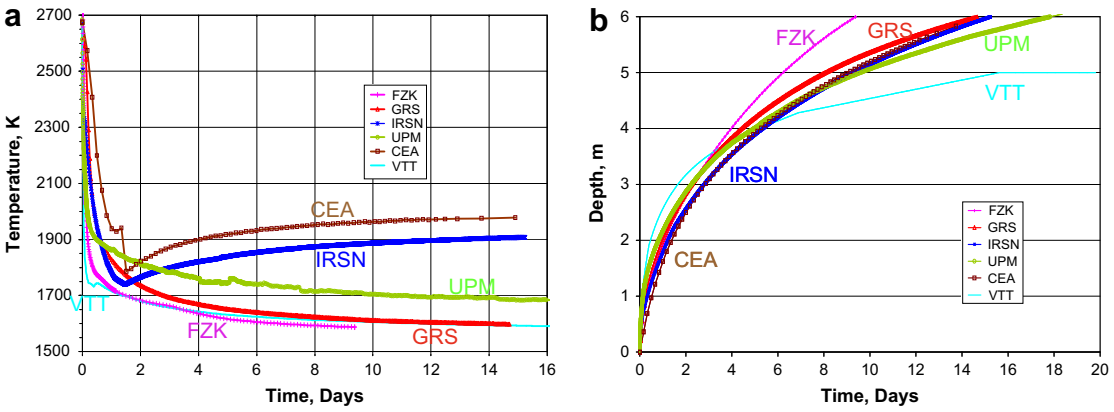

pool temperature versus time

axial ablation depth versus time

Fig. 4. Reactor benchmark, homogeneous pool, limestone concrete.

between 4 and 5.5 days; a larger scattering appears at later times on the axial ablation. Similar cavity shapes are found with lateral and axial ablations close to each other.

5.3. Homogeneous pool, siliceous concrete

Some results are presented in Fig. 5. Again the bulk pool temperature differences (Fig. 5a) are reflecting the different choices for the melt/crust interface. The scatter is around 300 K. The temperature increase in the CEA curve is an artefact due to the GEMINI coupling. Differences in axial ablation start earlier than for limestone concrete and amplify with time. However similar cavity shapes with a nearly isotropic ablation are found by the codes in case of siliceous concrete except for MELCOR with a smaller radial ablation.

The ablation rates (Fig. 5b) depend on the heat transfer models at the top surface and at the interfaces between pool and concrete: heat transfer coefficients and interface temperatures. In case of a siliceous concrete, the models selected in the different codes lead to larger deviations compared to LCS concrete. In other words the larger deviations are due to the larger uncertainty in two-dimensional ablation for siliceous concrete. Furthermore the anisotropy observed in CCI tests (Farmer et al., 2007) and VB-U5 test (Journeau et al., 2008b) for siliceous concrete was not modeled excepted by CORQUENCH code and, if taken into account, would increase still more the scatter between results.

5.4. Stratified pool, limestone concrete

Some results are presented in Fig. 6.

5.4.1. Stratification

A fixed stratified configuration is used in case of FZK (WECHSL) and GRS (ASTEC). For IRSN (ASTEC) the pool is first stratified with metal above, then the pool is mixed when the density of the layers are close, and the pool is stratified again with metal at the bottom; for IRSN (ASTEC), the stratified regime stops at about 1.4 days, when all metal is oxidized; this occurs because the additional metal brought by concrete ablation is oxidized immediately due to a sufficient gas inlet flow-rate.. For CEA (TOLBIAC), the pool is first homogeneous due to the high initial gas flow rate; when the BALISE criterion is reached in this calculation (low gas flow rate, high density difference), there is not enough metal any more to allow stratification and the pool remains homogeneous, and the results are the same as those obtained with the homogeneous pool.

5.4.2. Pool temperatures

The oxide layer temperature (Fig. 6a) is again dependent on the model used for the pool/crust interface. In the stratified regime with metal at the bottom, the bulk metal temperature (Fig. 6b) is either higher or lower than the oxide temperature depending on the code. Metal solidification is predicted before one day by FZK

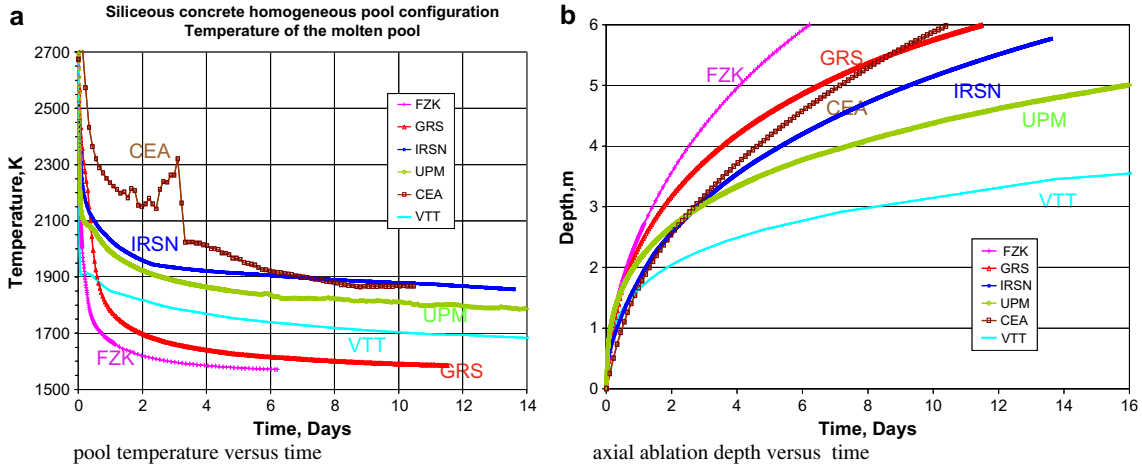

pool temperature versus time

axial ablation depth versus time

Fig. 5. Reactor benchmark, homogeneous pool, siliceous concrete.

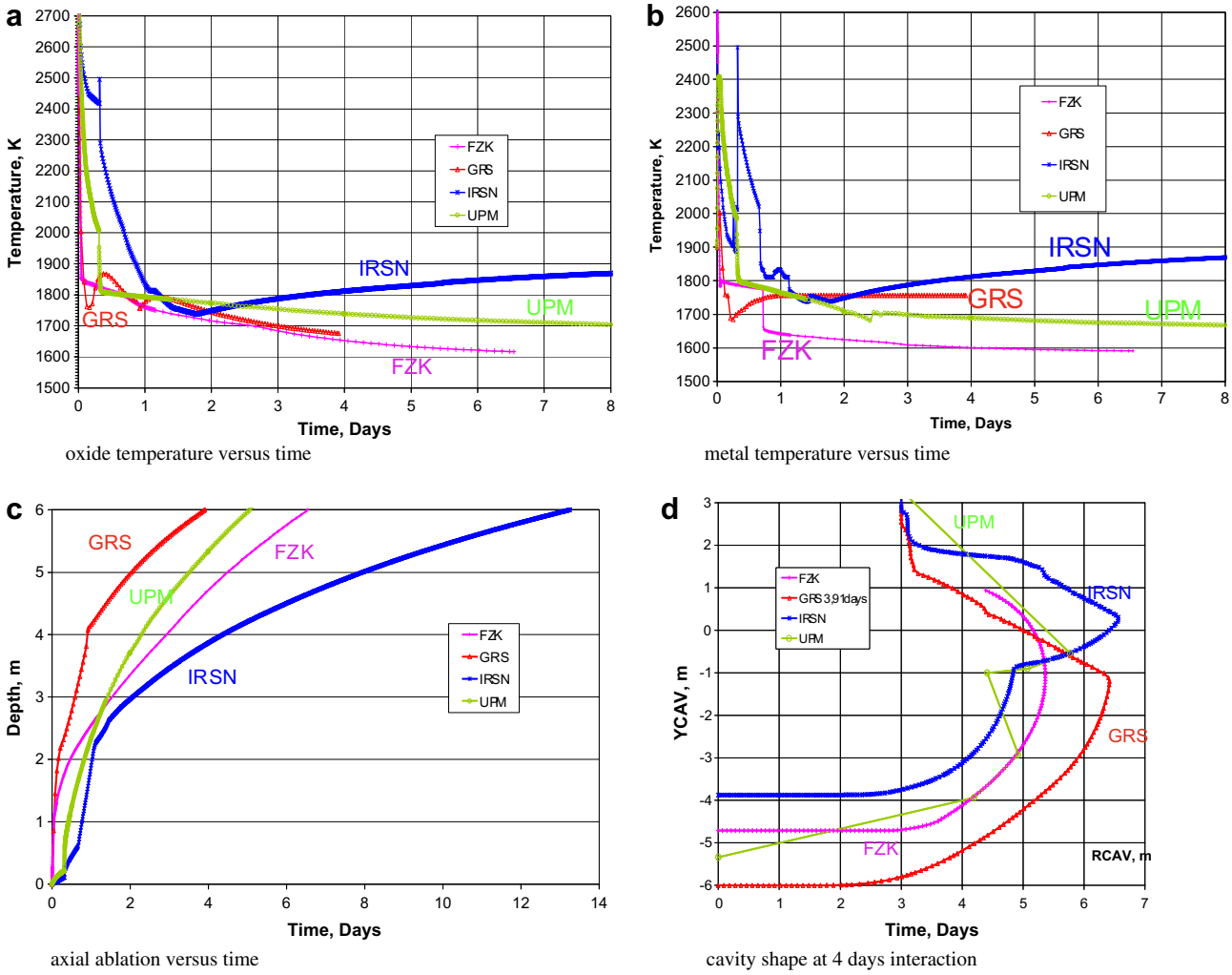

oxide temperature versus time

metal temperature versus time

axial ablation versus time

cavity shape at 4 days interaction

Fig. 6. Reactor benchmark, stratified pool, limestone concrete.

(WECHSL). For the other codes, it is delayed or hindered, due to the high heat transfer exchange between oxide and metal layers.

5.4.3. Concrete ablation and cavity shape

Compared to the case with a homogeneous melt, a larger scattering in axial ablation results is observed. The axial ablation (Fig. 6c) reaches 4 m within 0.8–4.5 days and 6 m within 3.7–13 days. The specific cavity shape (Fig. 6d) obtained by IRSN (ASTEC) and UPM (MELCOR) is due to the initial stratified configuration with metal above: the decay power is focussed from the oxide layer to the metal layer located above and hence to the lateral metal/concrete interface causing a large initial lateral cavity expansion. At the opposite, the initial axial ablation (Fig. 6c) is faster in case of a fixed stratified metal/oxide configuration with metal at the bottom from the beginning. The less axially elongated cavity (Fig. 6d) in FZK (WECHSL) calculation compared to GRS (ASTEC) is explained by the lower oxide/metal heat transfer coefficient used by WECHSL.

5.5. Stratified pool, siliceous concrete

Some results are presented in Fig. 7.

5.5.1. Stratification

With siliceous concrete, the oxidation of the metal layer is slower due to a lower gas release. For CEA (TOLBIAC), stratification occurs at about 0.6 days and the pool remains in a stratified configuration. For IRSN also (ASTEC), stratification with metal layer below occurs at 0.43 day and the pool remains stratified until melt-through time.

5.5.2. Pool temperatures

The scatter in oxide temperatures (Fig. 7a) and metal temperatures (Fig. 7b) is very large (600 K at 2 days). Again in the stratified regime with metal at the bottom, the bulk metal temperature is either higher or lower or close to the oxide temperature depending on the code and metal solidification is predicted at about one day by FZK (WECHSL). The sudden variation of the metal temperature by IRSN (ASTEC) is due the switch from a stratified pool to a mixed oxide/metal pool and backwards. The rather high metal temperature for CEA (TOLBIAC) is due to the bottom layer composition given by GEMINI, with about 8% weight fraction oxide and 92% metal.

5.5.3. Concrete ablation and cavity shape

Three results give an axial melt through at about 2 days (Fig. 7c), even if the shape of the cavity at this time is different (Fig. 7d). The specific cavity shape obtained by IRSN (ASTEC) and UPM (MELCOR) is again due to the initial stratified configuration with metal above. The effect of the interlayer heat transfer coefficient is clear: when it is high (GRS, IRSN, UPM), a large part of the decay heat is transferred to the bottom metal layer, and the bottom ablation is

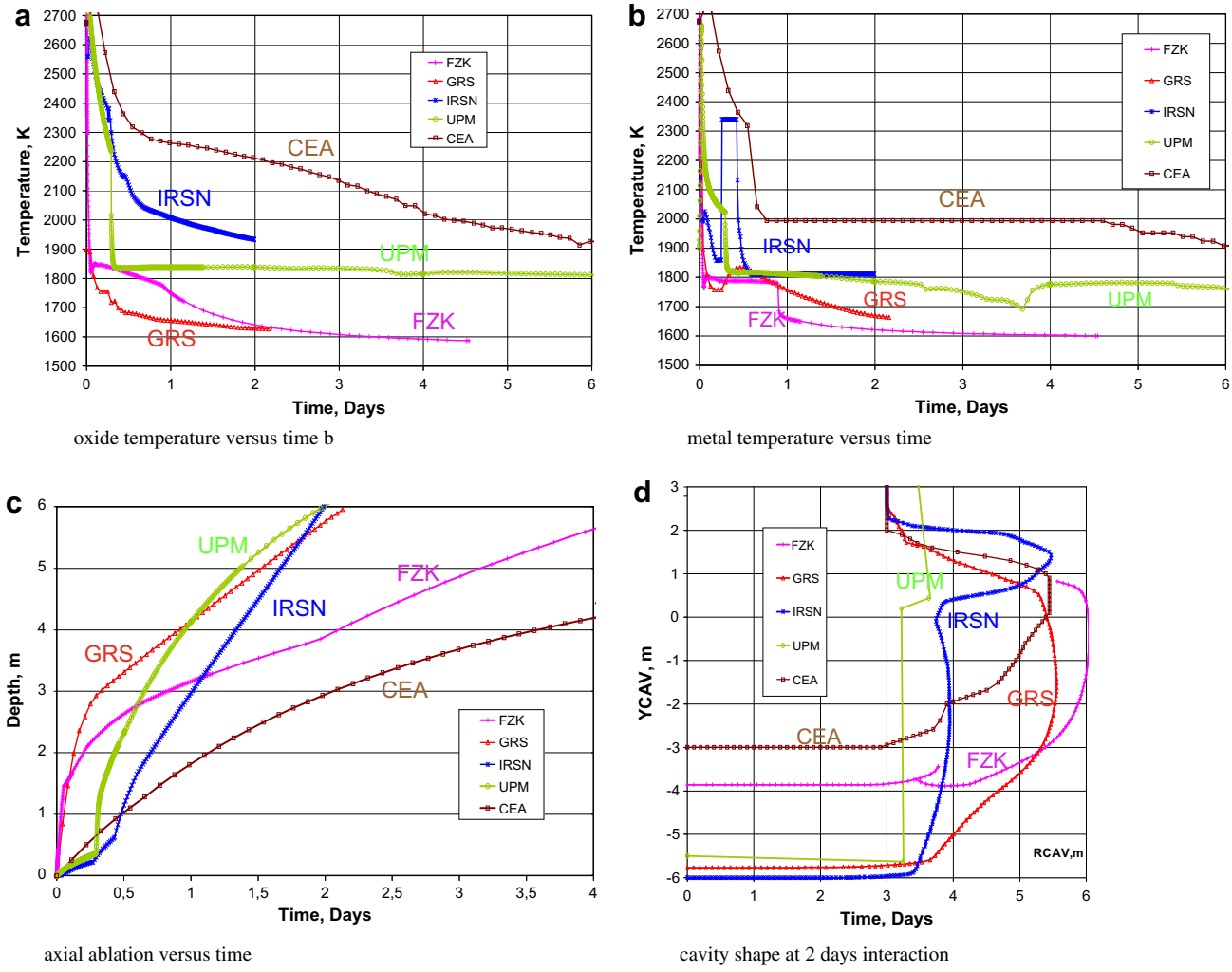

Fig. 7. Reactor benchmark, stratified pool, siliceous concrete.

increased. When it is low, the bottom ablation in the metal layer is reduced and the melt through time is largely increased (about 6 times between IRSN and CEA). Compared to the situation with limestone concrete, the bottom ablation is faster for IRSN, because the configuration remains stratified.

6. Comparison of the benchmarks results

The interest of the benchmarking work presented here is that the same input data are used by the participants, even if, in case of CCI-2, it is not the final experimental data.

What can be examined here is the consistency between code assumptions used for experiments and those retained for reactor cases, the reactor predictions being the purpose of the codes development.

6.1. Homogeneous configuration

Concerning the homogeneous configuration, the first difference concerns the initial interaction. Before a steady state regime is reached, peculiarities depending on the initial temperature and on the heating process exist in the experiments. These effects are more or less well simulated with the codes, depending on the model (liquidus or solidus at interface), but this is of minor importance, since for the reactor cases the initial effects are not significant compared to the long term behaviour.

The second point is the common large scatter of the bulk temperature for the experiment and reactor benchmarks, depending on the pool/crust interface model used: either close to liquidus or to solidus. However, the codes validation matrix now includes the CCI-2 test, and they are able to calculate the CCI-2 bulk temperature. The difference with the result of the benchmark is that they use the modified final input data, or also some fitting of the heat transfer parameters for GRS with ASTEC (Spengler et al., 2005), for IRSN with ASTEC (Cranga et al., 2008), for CEA with TOLBIAC-ICB (Spindler and Dufour, 2007). But the consequence is that for the reactor case the same models have to be used as those used for the experimental cases. Nevertheless, in spite of the fitting of model parameters against the CCI-2 test, significant code deviations on the bulk temperature appear at least in the long term phase in the reactor cases even with a homogeneous pool and limestone concrete as in CCI-2.

As far as ablation rate is concerned, the main issue here is the distribution of the input power between the upper pool surface, the side concrete interface and the bottom concrete interface. For CCI-2, an isotropic power split corresponds to the experiment, but we know it is not the case for siliceous concrete for the CCI tests (Farmer et al., 2007), for the VULCANO tests (Journeau et al., 2008a). This power split is one of the major uncertainties that are not yet solved for MCCI, even if some new perspectives are now proposed (Cranga et al., 2008; Seiler and Tourniaire, 2008; Journeau et al., 2008b).

6.2. Stratified configuration

Concerning the stratified configuration, the comparison between the COMET-L2-L3 benchmark and the reactor benchmark is not completely suitable, because the input power is not located in the same layer, and there is no modification of the pool configuration during the tests. However, the scatter concerning the bulk temperature, and the axial and radial ablations calculated by codes for the COMET-L experiments is quite large.

A second major uncertainty concerns the heat transfer coefficient between two stratified layers: is it higher than the pool/wall heat transfer coefficient, or of the same order of magnitude? In case it is higher, the axial melt through will be promoted all the more as the switch to a stratified pool with metal below occurs early and the metal layer remains present in the longer term in spite of oxidation.

7. Conclusion

The recent benchmarking work concerning corium concrete interaction in 2D geometry is summarized: CCI-2 test, COMET-L2 and COMET-L3 tests in the frame of SARNET, and finally the reactor case benchmarking work performed by SARNET partners and analysed through a SARNET mobility detachment. A large scatter is found concerning the bulk temperature, which is related to the interfacial model between pool and crust: interfacial temperature close either to the liquidus or to the solidus. Concerning the lateral and axial ablations, it depends on the model or directly on the choice of the code user. A global consistency is then reached between the experiment and reactor case.

The major uncertainties that are pointed out in these analyses concern mainly the pool/concrete interface model and the heat flux distribution along lateral and bottom interfaces in case of a fixed homogeneous pool configuration. In case stratification is allowed, they concern the initial pool configuration assumptions and subsequent configuration evolution models, and the interlayer heat transfer.

The benchmark analyses presented here show consequently the high interest of further work concerning modelling and code validation against available 2D MCCI experiments, as well as a performance of additional real material experiments with siliceous concrete, where code discrepancies are larger and axial ablation kinetics may be faster.

Finally this benchmark work contributed largely to define the content of the SARNET2 WP6 Work Programme, which is focused on still pending questions about MCCI, in particular for sub-packages WP6.1 and WP6.2.

Acknowledgement

The research leading to these results has received funding from the European Atomic Energy Community's Sixth Framework Programme area "Nuclear Fission: Safety of Existing Nuclear Installations", under contract number FI6O-CT-2004-509065.

References

Allelein, H.J., Bürger, M., 2006. Considerations on Ex-Vessel corium behavior: scenarios, MCCI and coolability. Nuclear Engineering and Design 236, 2220–2236.

Alsmeyer, H., Cron, T., Fluhrer, B., Messemer, G., Miassoedov, A., Schmidt-Stiefel, S., Wenz, T., 2007. The COMET-L3 experiment on Long-Term Melt-Concrete Interaction and cooling by surface flooding, Forschungszentrum Karlsruhe, Wissenschaftliche Berichte, FZKA 7244.

Bonnet, J.M., 2000. Thermal hydraulic phenomena in corium pools for ex-vessel situations: the BALI experiment. In: Proceedings of ICONE8, Baltimore, USA, April 2–6.

Cheynet, B., Chaud, P., Chevalier, P.Y., Fischer, E., Mason, P., Mignanelli, M., 2004. NUCLEA "propriétés -dynamiques et équilibres de phases dans les systèmes d'intérêt nucléaire" Journal de Physique IV 113, 61–64. France.

Cranga, M., Fabianelli, R., Jacq, F., Barrachin, M., Duval, F., 2005. The MEDICIS code, a versatile tool for MCCI modelling, International Congress on Advances in Nuclear Power Plants, Seoul, Korea, May 15–19, Paper 5416.

Cranga, M., Michel, B., Duval, F., 2007. Relative impact of MCCI modeling uncertainties on reactor basemat ablation kinetics, MCCI-OECD Project Seminar, Cadarache, France.

Cranga, M., Mun, C., Michel, B., Duval, F., Barrachin, M. 2008. Interpretation of real material 2D MCCI experiments in homogeneous oxidic pool with the ASTEC/MEDICIS code. In: Proceedings of ICAPP08, Paper 8098, Anaheim, California, USA.

Farmer, M.T., 2001. Modeling of ex-vessel corium coolability with the CORQUENCH code. In: Proceedings of ICONE9 Conference. Nice, France.

Farmer, M.T., Lomperski, S.W., Basu, S. 2005. The results of the CCI-2 reactor material experiment investigating 2-D core-concrete interaction and debris coolability, NURETH-11, Paper 245, Avignon, France.

Farmer, M.T., Lomperski, S., Kilsdonk, D., Aeschlimann, R., 2007. A summary of findings from the Melt Coolability and Concrete Interaction (MCCI) Program. In: Proceedings of ICAPP 2007, Paper 7544. Nice, France.

Foit, J.J., 1997. Modeling oxidic molten core-concrete interaction in WECHSL. Nuclear Engineering and Design 170, 73–79.

Foit, J.J., 2007. Overview and history of core concrete interaction issues (international review), MCCI Project Seminar, Cadarache, France.

Gauntt, R.O., Cash, J.E., Cole, R.K., Erickson, C.M., Humphries, L.L., Rodriguez, S.B., Young, M.F., 2005. MELCOR Computer Code Manuals. Sandia National Laboratories. NUREG/CR 6119, SAND2005-5713.

Greene, G.A., Irvine, T.F., 1988. "Heat transfer between stratified immiscible liquid layers driven by gas bubbling across the interface". In: ANS Proceedings of the National Heat Transfer Conference, Houston, TX.

Journeau, C., Bonnet, J.M., Boccaccio, E., Piluso, P., Sevon, T., Pankakoski, P.H., Holmström, S., Virta, J., 2008a. Current European Experiments on 2D molten core concrete interaction: HECLA and VULCANO. In: Proceedings of ICAPP08, Paper 8058, Anaheim, California, USA.

Journeau, C., Haquet, J.F., Piluso, P., Bonnet, J.M., 2008b. Differences between silica and limestone concretes that may affect their interaction with corium. In: Proceedings of ICAPP08, Paper 8059, Anaheim, California, USA.

Kutateladze, S.S., Malenkov, I.G., 1978. Boiling and bubbling heat transfer under the conditions of free and forced convection. In: 6th International Heat Transfer Conference, Toronto.

Langhans, J., Spengler, C., Druwe, H., 2001. ASTEC V1-Description of WEX3.1 Rev0, Report ASTEC-V1/DOC/01–33, GRS and IRSN.

Nie, M., Fischer, M., Lohnert, G., 2002. Advanced MCCI modelling based on stringent coupling of thermal hydraulics and real solution thermochemistry in COSACO. In: Proceedings 10th International Conference on Nuclear Engineering (ICONE 10), Arlington, VA.

Roche, M.F., Leibowitz, L., Fink, J.K., Baker, L. Solidus and liquidus temperatures of core-concrete mixtures, US regulatory Commission Report NUREG/CR-6032, ANL Report ANL-93/9, 1993.

Sdouz, G., Mayrhofer, R., Alsmeyer, H., Cron, T., Fluhrer, B., Foit, J., Messemer, G., Miassoedov, A., Schmidt-Stiefel, S., Wenz, T., 2006. The COMET-L2 Experiment on Long-Term MCCI with Steel Melt, Forschungszentrum Karlsruhe, Wissenschaftliche Berichte, FZKA 7214 and SAM-LACOMERA-D15.

Seiler, J.M., Tourniaire, B., 2008. Towards a comprehensive interpretation of MCCI 2D tests. In: Proceedings of ICAPP08, Paper 8141, Anaheim, California, USA.

Spengler, C., Allelein, H.J., Cranga, M., Duval, F., Van Dorsselaere, J.P., 2005. Assessment and development of molten corium concrete interaction models for the integral code ASTEC. In: Proceedings of EUROSAFE meeting, Brussels, Belgium.

Spindler, B., Dufour, E., 2007. Simulation of the CCI-2 test with TOLBIAC-ICB: modeling and sensitivity studies, MCCI-OECD Project Seminar, Cadarache, France.

Spindler, B., Tourniaire, B., Seiler, J.M., 2006. Simulation of MCCI with the TOLBIAC-ICB code based on the phase segregation model. Nuclear Engineering and Design 236, 2264–2270.

Spindler, B., Atkhen, K., Cranga, M., Foit, J., Garcia, M., Schmidt, W., Sevon, T., Spengler, C., 2007a. Simulation of molten corium concrete interaction in a stratified configuration: the COMET-L2-L3 Benchmark, European Review Meeting on severe Accident Research (ERMSAR07), Paper S2-5, Karlsruhe.

Spindler, B., Atkhen, K., Cranga, M., Fischer, M., Kawabe, R., Kim, H.Y., Ley, H., Rydl, A., Spengler, C., 2007b. Simulation of molten corium concrete interaction: the CCI-2 benchmark organized in the frame of the OECD-MCCI Project, MCCI Project Seminar, Cadarache, France.

Tourniaire, B., Seiler, J.M., Bonnet, J.M., 2003. Study of the mixing of immiscible liquids: results of the BALISE experiments. In: Proceedings of NURETH-10, Seoul, Korea.

Werle, H., 1982. Enhancement of heat transfer between two horizontal liquid layers by gas injection at the bottom. Nuclear Technology 59, 160–164.